

1 **Supplemental Information:**

2 **Pan, et al., Prostate tumor-derived GDF11 accelerates androgen deprivation**
3 **therapy-induced sarcopenia**

4
5 **Supplemental Methods**

6 *RNA isolation and quantitative RT-PCR.* Tissues were harvested after euthanasia, snap
7 frozen in liquid nitrogen, and stored at -80°C for mRNA expression analysis. Total RNA
8 was extracted from pulverized QUA or tumor tissue using TRIzol (Invitrogen). Five
9 micrograms of total RNA were reverse transcribed using pdN15 with the Superscript III
10 reverse transcription kit (Invitrogen, Waltham, MA, USA) to generate single-strand cDNA.
11 PCR was performed using SYBR[®] Green qPCR Master Mix (Molecular Probes, Eugene,
12 OR, USA) in a StepOnePlus instrument (Applied Biosystems, Waltham, MA, USA). PCR
13 primers, spanning at least one intron are listed in Supplemental Table S3. Standard
14 curves were generated using linearized plasmids encoding the corresponding cDNAs to
15 assure linearity of quantitation. The mean expression levels of the combination of
16 GAPDH and eEf2 (eukaryotic elongation factor 2) were used to normalize target gene
17 expression for total cDNA input from tumor tissue. The mean expression levels of
18 ribosomal protein L32 were used to normalize target gene expression for total cDNA input
19 from QUA muscle tissue. RNA from tissues from at least three mice, each reverse
20 transcribed three times, were analyzed, and qPCR was performed in triplicate for each
21 sample.

22 *Mouse assessments.* Total body mass absent tumor was calculated using total body mass
23 by weighing less the mass of the tumor, estimated as 1 mg per cubic millimeter tumor volume
24 for correlative analysis in Supplemental Fig. S3.

26 **Supplemental Discussion**

27 TGF β -family proteins exist largely in a latent pro-domain or inhibitor-bound form
28 and the active, soluble dimeric TGF β -family myokines represent a small proportion of the
29 overall protein (1, 2). Therefore, measurement of functional ligands requires that soluble
30 active TGF β -family myokines be examined using dimer-specific assays (3). Active
31 myostatin c-terminal dimer was measured using a specific immunoblot assay, since
32 available ELISA assays do not discriminate this form from latent pro-domain or inhibitor-
33 bound myostatin c-terminal dimer (4). Dimer-specific ELISA assays used for each of the
34 activins and GDF11, and the myostatin immunoblots, demonstrated distinct patterns of
35 induction for each catabolic myokine in muscle after castration (Fig. 3). Measurement of
36 myostatin and GDF11 has been problematic due to protein homology (5, 6). In muscle,
37 serum, and tumor, the patterns of myostatin and GDF11 expression were distinct (Figs.
38 3 and 5). Similarly, the function-neutralizing anti-GDF11 monoclonal antibody employed
39 did not cross-react with myostatin (Supplemental Fig. S8). The observed ADT-regulation
40 of soluble active myostatin c-terminal dimer levels and soluble GDF11 are also distinct
41 from the ADT-unregulated and quantitatively ~100-fold higher levels of total acid-
42 solubilized myostatin (Supplemental Fig. S9). These data strongly suggest specific
43 measurement of the castration-induced expression level changes of the active dimers of
44 activins, myostatin, and GDF11, and specific neutralization of circulating GDF11.

45

46

47
48
49
50
51
52
53
54
55
56
57
58
59
60
61
62
63
64
65

References

1. Lee SJ. Extracellular Regulation of Myostatin: A Molecular Rheostat for Muscle Mass. *Immunol Endocr Metab Agents Med Chem.* 2010;10:183-194.
2. Hill JJ, et al. The myostatin propeptide and the follistatin-related gene are inhibitory binding proteins of myostatin in normal serum. *J Biol Chem.* 2002;277(43):40735-41.
3. Rodgers BD. The Immateriality of Circulating GDF11. *Circ Res.* 2016;118(10):1472-4.
4. Anderson SB, Goldberg AL, and Whitman M. Identification of a novel pool of extracellular pro-myostatin in skeletal muscle. *J Biol Chem.* 2008;283(11):7027-35.
5. Egerman MA, et al. GDF11 Increases with Age and Inhibits Skeletal Muscle Regeneration. *Cell Metab.* 2015;22(1):164-74.
6. Schafer MJ, et al. Quantification of GDF11 and Myostatin in Human Aging and Cardiovascular Disease. *Cell Metab.* 2016;23(6):1207-15.

66 **Supplemental Table S1. Analysis of tumor volume correlation with physiological assessments.**
 67 Regression analysis for tumor-bearing cohort #1 of weekly measures of tumor volume versus initial pre-
 68 castration tumor volume, and grip strength and total body mass versus tumor volume at the week of
 69 assessment.
 70

A: Post-castration tumor volumes versus initial (pre-castration) tumor volume

Relevant to supplemental Fig. S3A

Week	n	slope (% change/1000 mm ³)	Pearson Correlation ('r')	p-Value
wk2	12	-13.4	0.451	0.141
wk4	12	-16.1	0.409	0.186
wk5	12	-21.3	0.476	0.117
wk7	12	-19.5	0.386	0.215
wk8	12	-26.4	0.489	0.106
wk9	12	-22.2	0.496	0.101
wk10	12	-29.9	0.626	0.029
wk14	12	-24.5	0.472	0.121
wk16	12	-27	0.578	0.049

B: Grip strength versus tumor volume at that same week

Relevant to supplemental Fig. S3B

Week	n	slope (N/ml)	Pearson Correlation ('r')	p-Value
wk2	12	-0.032	0.164	0.610
wk4	12	-0.033	0.167	0.603
wk5	12	-0.056	0.342	0.277
wk7	12	-0.043	0.210	0.513
wk8	12	-0.047	0.173	0.590
wk9	12	-0.035	0.237	0.459
wk10	12	-0.033	0.249	0.435
wk14	12	-0.008	0.095	0.769
wk16	12	-0.011	0.130	0.686

71
72

73 **Supplemental Table S2. Analysis of tumor volume correlation with end-point measures.** Regression
 74 analysis of final measures of individual skeletal muscle mass and body composition for tumor-bearing
 75 cohort #1 versus initial pre-castration tumor volume.

A: Body composition versus tumor volume after 16 weeks castration

Relevant to supplemental Fig. S3D, S3E

	n	slope (% change/1000 mm ³)	Pearson Correlation (r')	p-Value
%fat	12	-2.16	0.545	0.067
%fluid	12	0.52	0.065	0.841
%bone	12	0.04	0.277	0.383
%lean	12	1.7	0.599	0.040

B: Muscle mass versus tumor volume after 16 weeks castration

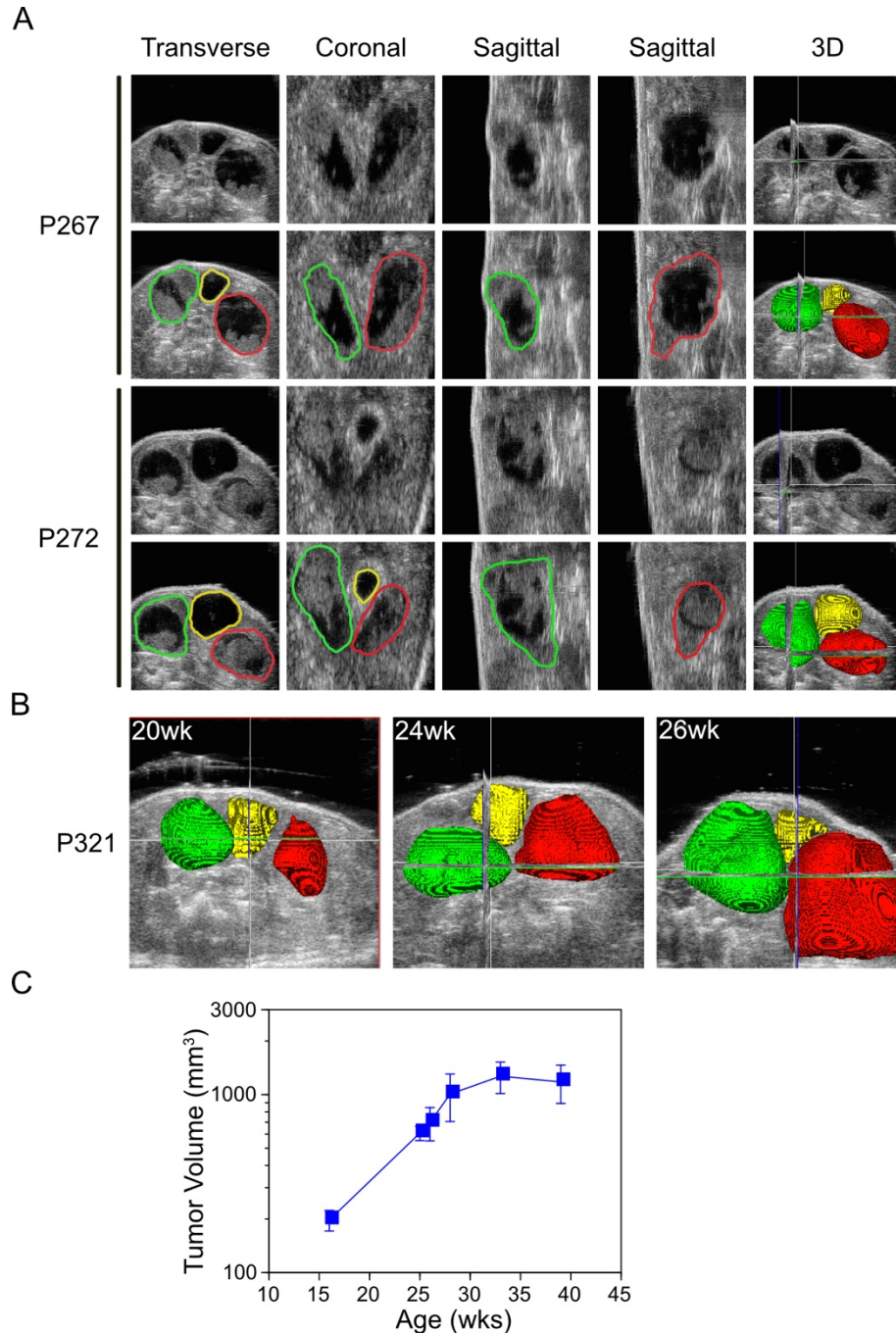
Relevant to supplemental Fig. S3F

	n	slope (% change/1000 mm ³)	Pearson Correlation (r')	p-Value
TA	12	-2.7	-0.287	0.366
EDL	12	-1.3	-0.198	0.537
SOL	12	-1.6	-0.358	0.253
GAS	12	-2.3	-0.080	0.805
QUA	12	11	0.328	0.298
TRI	12	-0.8	-0.033	0.926

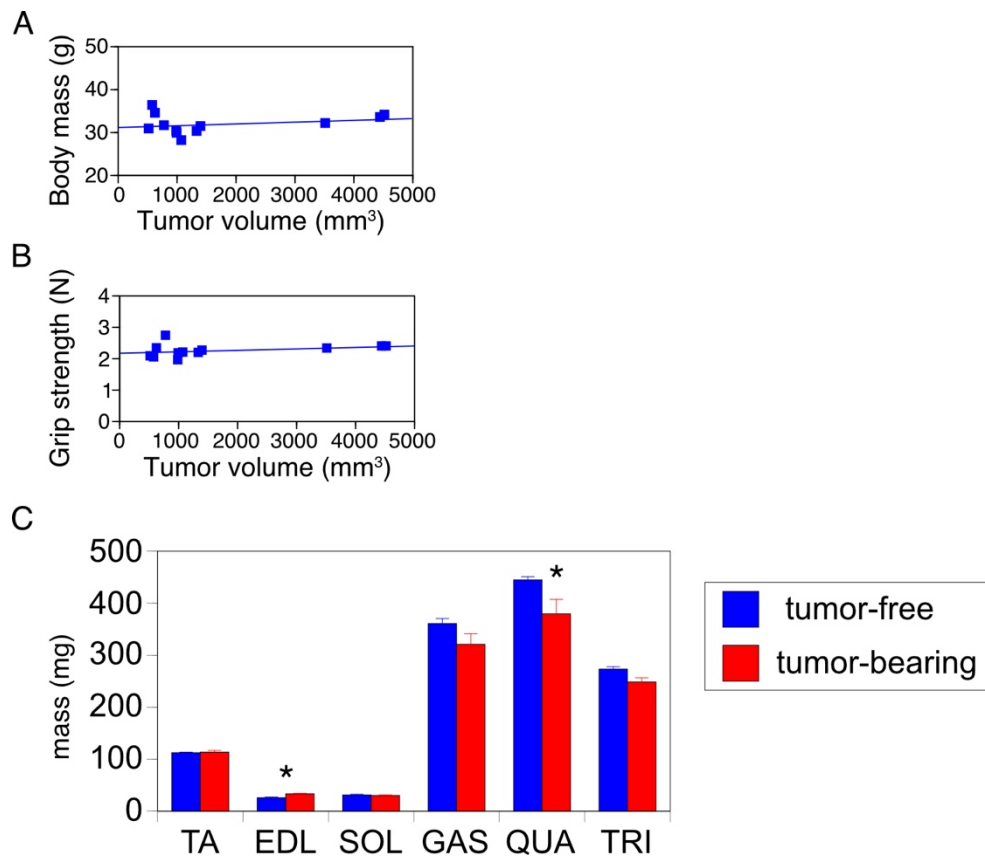
76
 77
 78 **Supplemental Table S3. Oligonucleotide primers used in qRT-PCR analysis.** Forward and reverse
 79 primers used to quantitate the indicated gene in RT-qPCR analyses.

80

Gene	Forward primer sequence	Reverse primer sequence
B-Actin	GCAGGAGTACGATGAGTCCG	ACGCAGCTCAGTAACAGTCC
EF2	TGCCTTGCGTGTCACCGATGGA	TCAGGACGGGCTTGATGCGTTGAG
GADPH	CTTTGGCATTGTGGAAGGGC	CAGGGATGATGTTCTGGGCA
RpL32	CCTGGTCCACAATGTCAAGGA	TGGGATTGGTACTCTGATGG
Atrogin-1	GTTCAAAAGGAAGTACGAAGG	AAGCTTTCAACAGACTGGACTTC
MuRF1	ACCTGCTGGTGGAAAACATC	AGGAGCAAGTAGGCACCTCA
Acvr1b	AAAGCCCTTCTACTGCCTGA	GATGATGCCGACCAGCTC
Acvr1c	GGCTGTGAAGCACGATTCTA	TCCAACCTGAACACCTTCGAG
Acvr2a	CGTTCGCCGTCTTTCTTATC	GCCCTCACAGCAACAAAAGT
Acvr2b	GTGGGAGCTCGTCTCTCG	GGTGTTCAGCCAGTGATCC
Inhibin Ba	GGAGATAGAGGACGACATTGGC	ACGCTCCACTACTGACAGGTCA
Inhibin Bb	CTCCGAGATCATCAGCTTTGCAG	GGAGCAGTTTCAGGTACAGCCA
GDF-11	TTTCGCCAGCCACAGAGCAACT	CTCTAGGACTCGAAGCTCCATG
Myostatin	AACCTTCCCAGGACCAGGAGAA	GGCTTCAAATCGACCGTGAGG

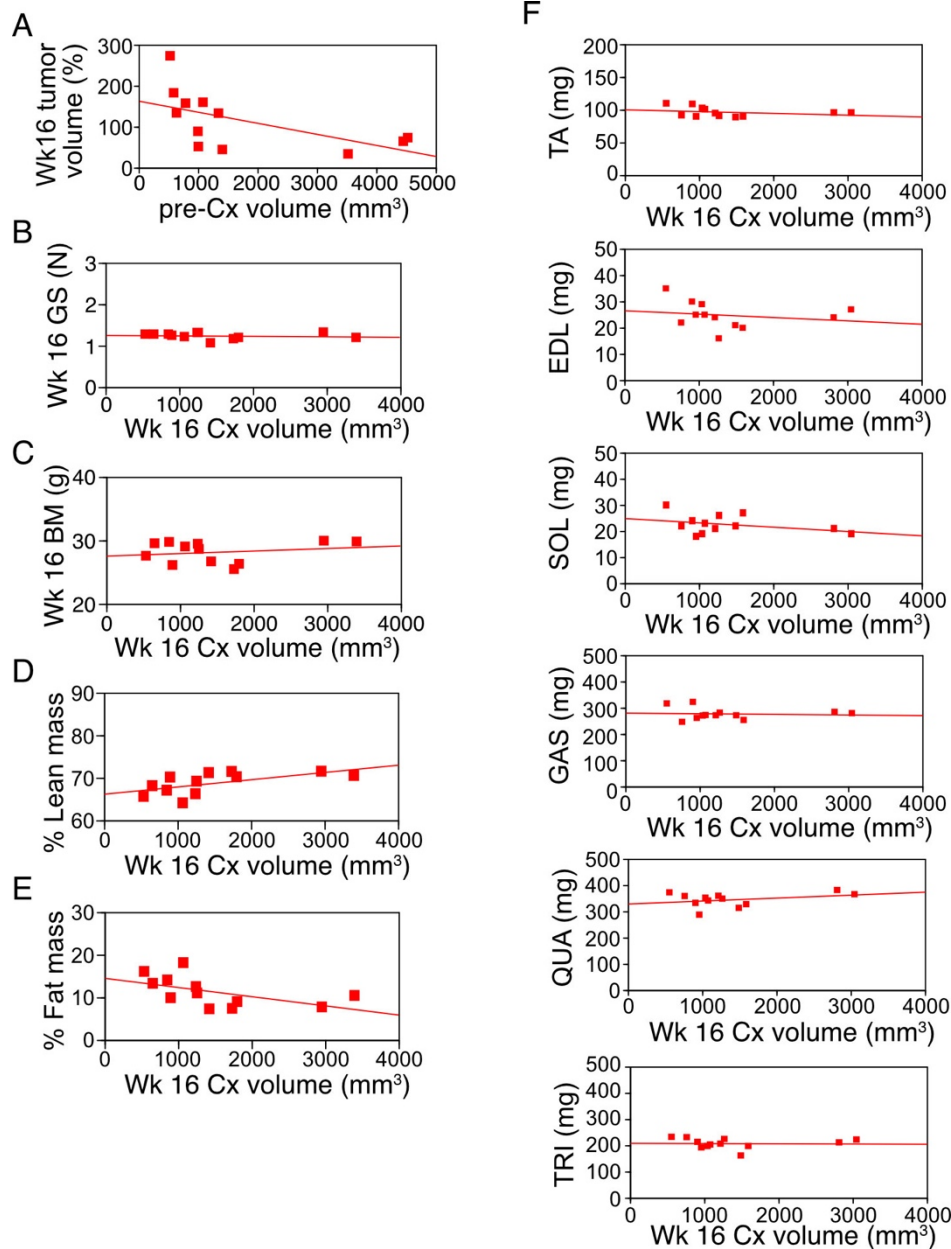


82
 83 **Supplemental Figure S1. High Frequency Ultrasound imaging (HFUS) with 3D reconstruction**
 84 **quantitated development of PTEN prostate KO tumor. (A)** Representative HFUS image slices of the
 85 genitourinary region from 2 PB-Cre4:Pten^{fl/fl} mice. Orthogonal planes (transverse, coronal and sagittal at each
 86 tumor lobe). The 3D image is an integrated reconstruction using Amira visualization. Bladder (yellow), left
 87 (green) and right (red) prostate tumor lobes. **(B)** Panels show Amira 3D reconstructions of HFUS images from
 88 a single PB-Cre4:Pten^{fl/fl} mouse over time. Leftmost illustrates tumor when the mouse is 20 wk (tumor volume
 89 = 215 mm³); Middle panel, at 24 wk (tumor volume = 387 mm³); Right panel at 26 wk (tumor volume = 730
 90 mm³) Colors as in **A**. **(C)** Growth of tumor volume in mice prior to analysis in Figure 1 (n=13). The later slowing
 91 of the overall mean growth rate was due to removal from the analysis of mice bearing the fastest-growing tumors
 92 as they were entered into the experimental protocol.



94
95
96
97
98
99
100
101
102
103
104

Supplemental Figure S2. Tumor burden did not influence total body mass, grip strength, or individual skeletal muscle mass. (A) Individual total body mass (BM), corrected for imputed tumor mass, was not correlated with tumor volume ($R^2=0.07$, $p=0.41$). (B) Grip strength (GS) was not correlated with pre-castration tumor volume ($R^2=0.12$, $p=0.28$). (C) Mass of TA, SOL, GAS, and TRI skeletal muscles from tumor-free mice (blue) did not differ from muscles from tumor-bearing mice (red). EDL was increased in tumor bearing mice, while QUA was decreased in tumor bearing mice ($*p<0.05$), determined using one-way ANOVA with Dunnett's test.



106

107

108

109

110

111

112

113

114

115

116

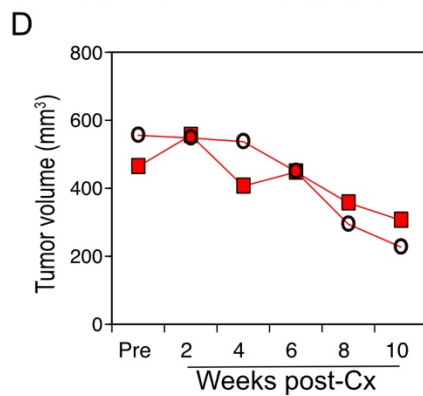
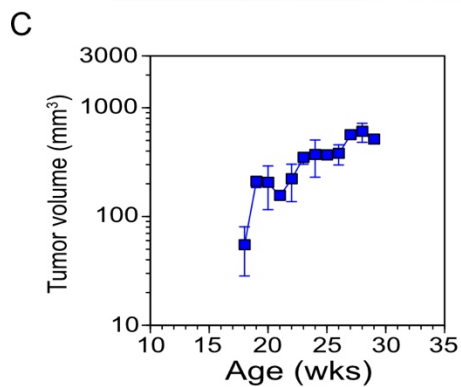
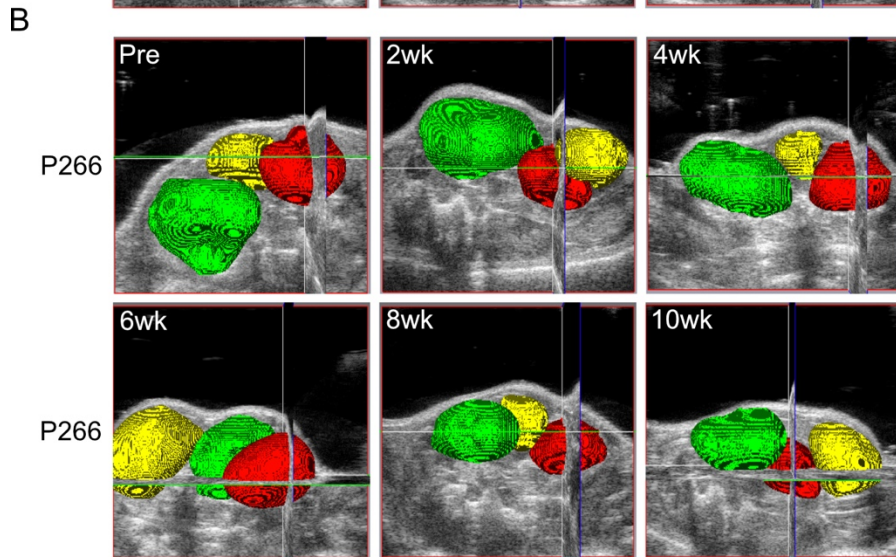
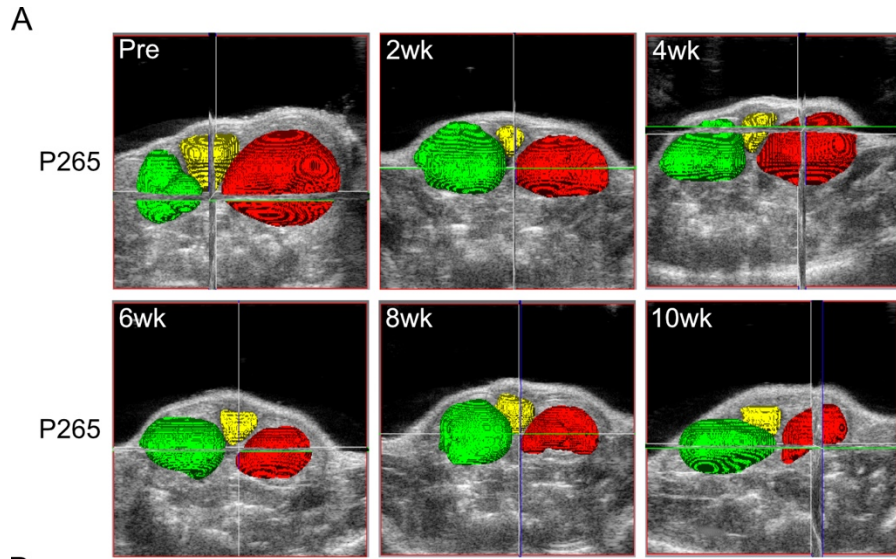
117

118

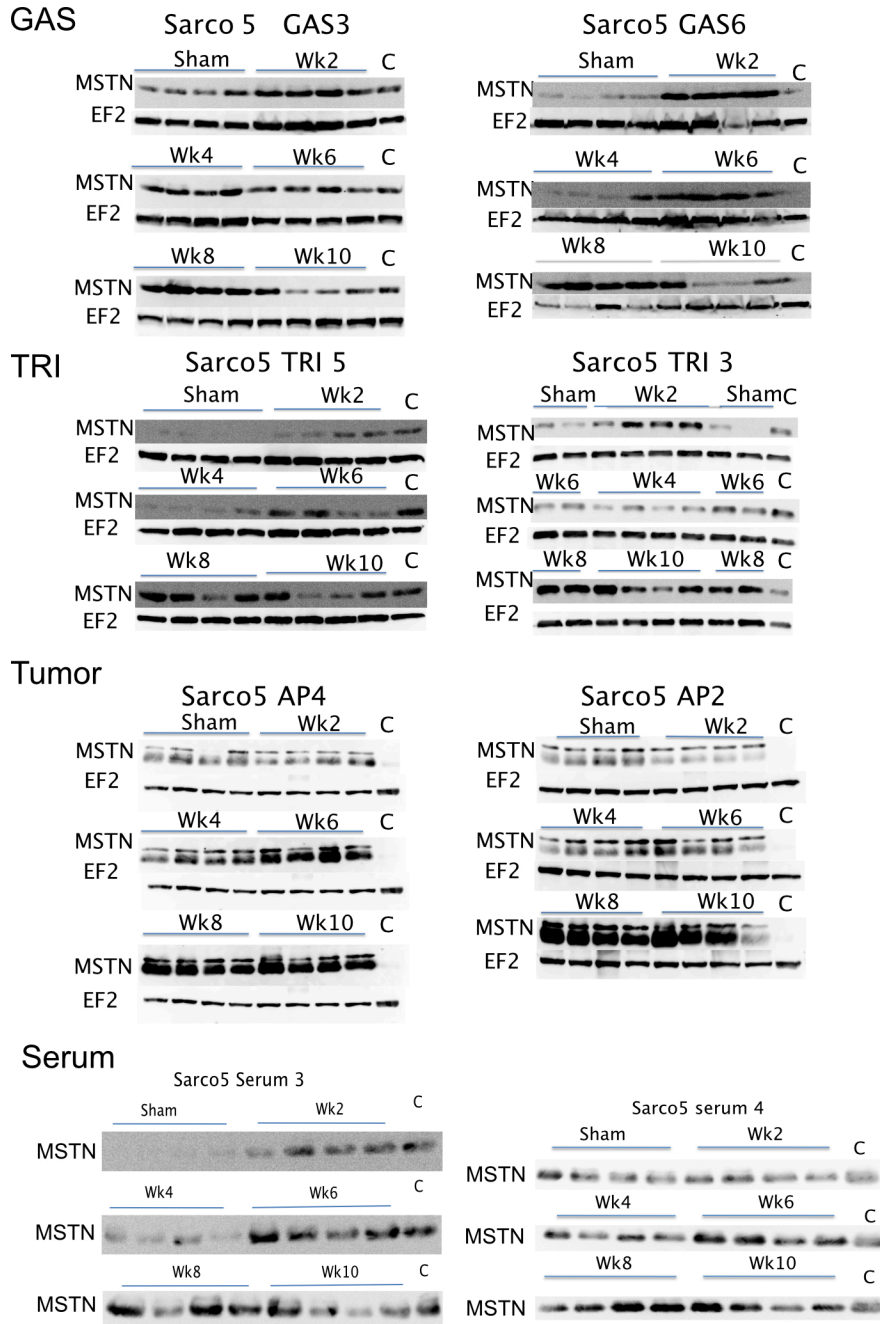
119

120

Supplemental Figure S3. Large tumors regressed more, but tumor burden did not alter grip strength, body mass, body composition, or skeletal muscle mass 16 weeks after castration. (A) Tumor regression (tumor volume as a percentage of initial volume) after 16 weeks castration (Cx) was negatively correlated ($\sim -25\%$ / 1000 mm^3) with pre-Cx tumor volume ($p=0.049$). (B) Grip strength (GS), in Newtons (N), was not correlated with tumor volume at any time up to 16 weeks after Cx. (C) Individual mean total body mass (BM), corrected for imputed tumor mass, was not correlated ($R^2=0.21$, $p=0.51$) with tumor volume 16 weeks after Cx. (D) Whole-body lean mass by qNMR (including tumor) increased 1.7% per 1000 mm^3 of increased tumor volume ($p=0.040$) 16 weeks after Cx. (E) Whole-body fat mass by qNMR was not correlated ($p=0.067$) with increased tumor volume 16 weeks after Cx. (F) Mass of individual skeletal muscles was not correlated with increased tumor volumes 16 weeks after Cx. Line indicates linear regression, $n=12$ for each muscle. See Supplemental Table S1 for intermediate time point (wk2-wk14) data, and Table S2 for end point data including slopes, Pearson correlations, and p-values.

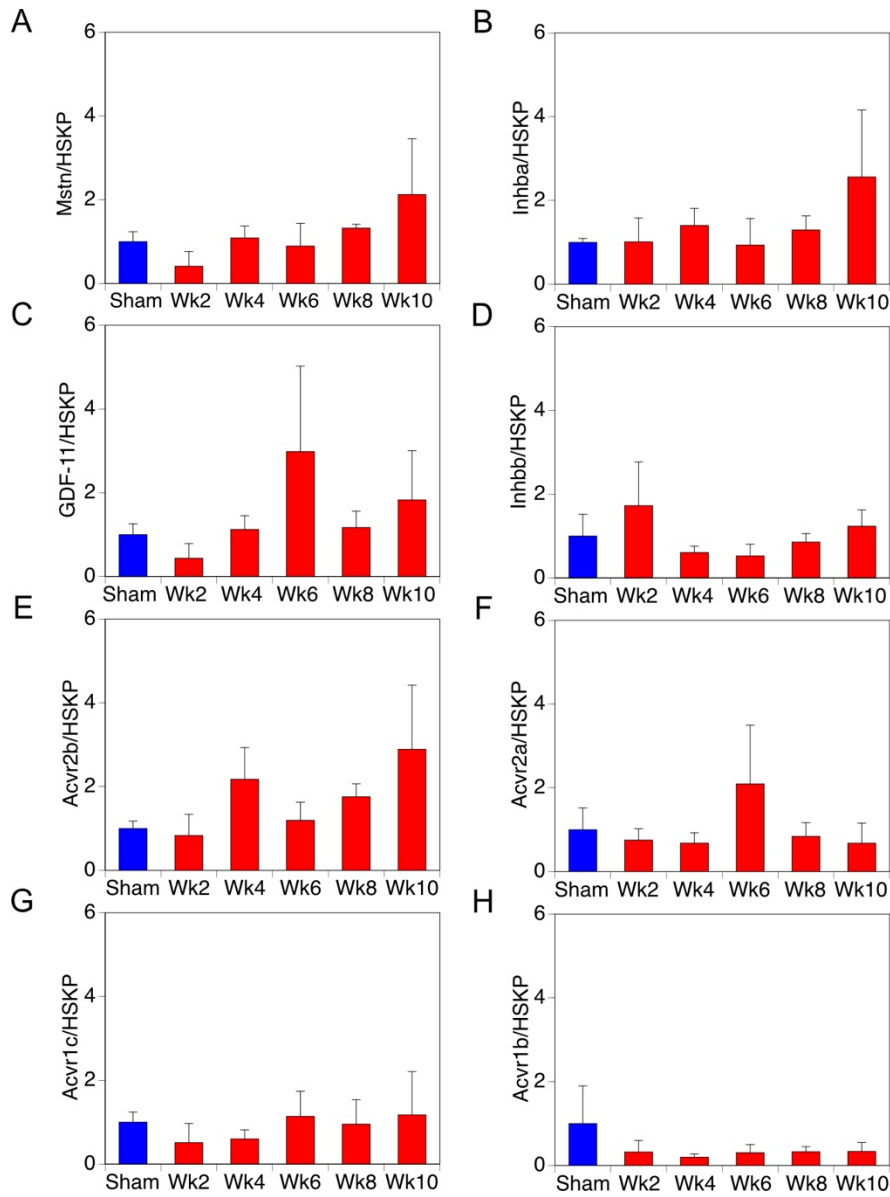


121
 122 **Supplemental Figure S4. High Frequency Ultrasound imaging with 3D reconstruction quantitated**
 123 **regression of PTEN prostate KO tumor. (A)** Panels show Amira 3D reconstructions of HFUS images of
 124 prostate tumor from a single PB-Cre4:Pten^{fl/fl} mouse imaged prior to castration (pre) and every two weeks for
 125 10 weeks after castration. Bladder (yellow), left (green) and right (red) prostate tumor lobes. **(B)** As in A. for a
 126 second tumor-bearing mouse. **(C)** Growth of tumor volume in mice prior to castration (n=12). **(D)** Quantitation
 127 of the tumor volumes of the mice depicted in each panel of **A**. (P265, open circles) and **B**. (P266, solid squares).
 128



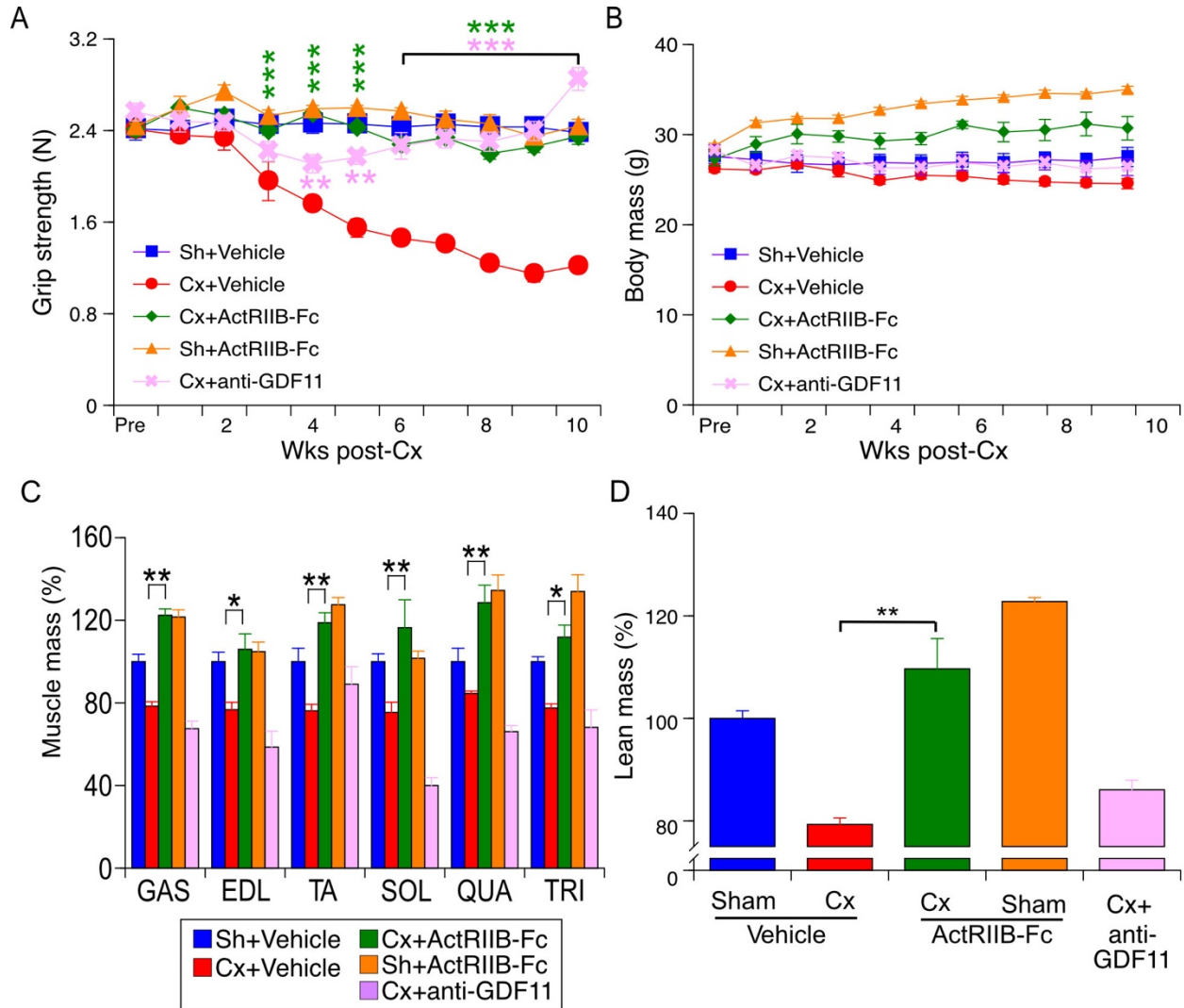
130
131
132
133
134
135
136
137
138
139

Supplemental Figure S5. Second and third replicates of immunoblots for myostatin quantitation in Figures 3 and 5. Images of the additional immunoblots of myostatin (MSTN), including eukaryotic elongation factor 2 (EF2) expression in prostate tumor tissue from sets of 4 mice, castrated for the indicated times or sham-castrated. Lanes of immunoblots marked “C” contain identical control sample for inter-blot comparison.

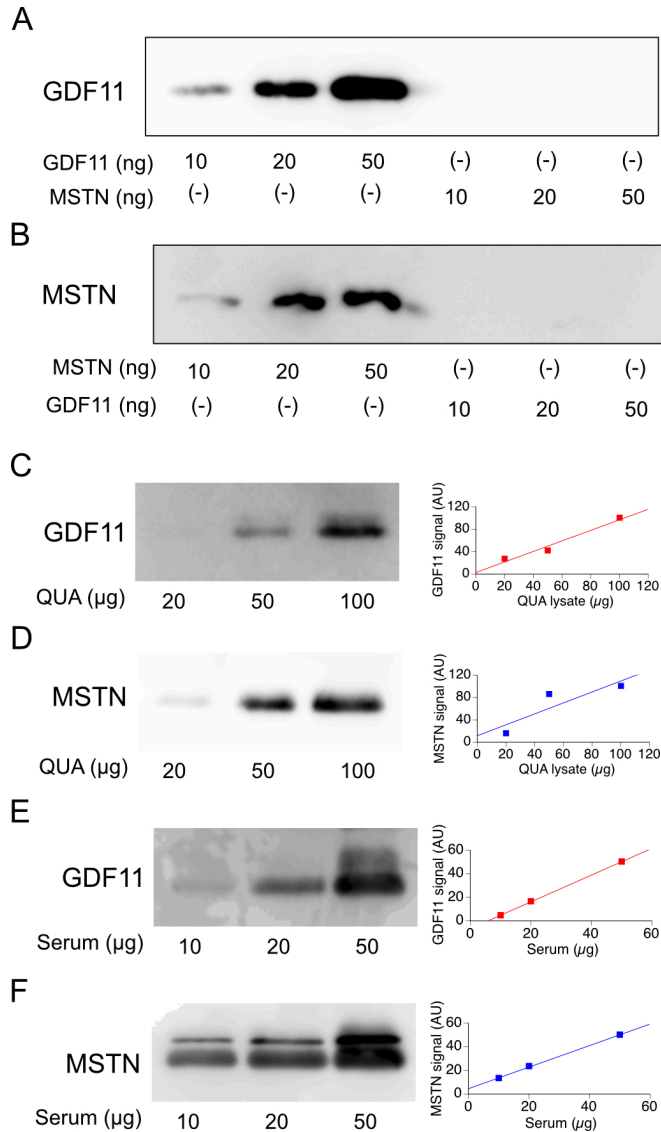


141
 142
 143
 144
 145
 146
 147

Supplemental Figure S6. Quantitation of TGFβ-family myokine related mRNAs in muscle. Expression of the indicated ligand and receptor mRNAs (A-H) from QUA muscle tissue of PTEN prostate KO mice sacrificed at the indicated number of weeks after castration. Expression of each gene was normalized to control (HSKP), and subsequently to the sham castrate expression levels, from 4 mice at each time, measured 3 times.

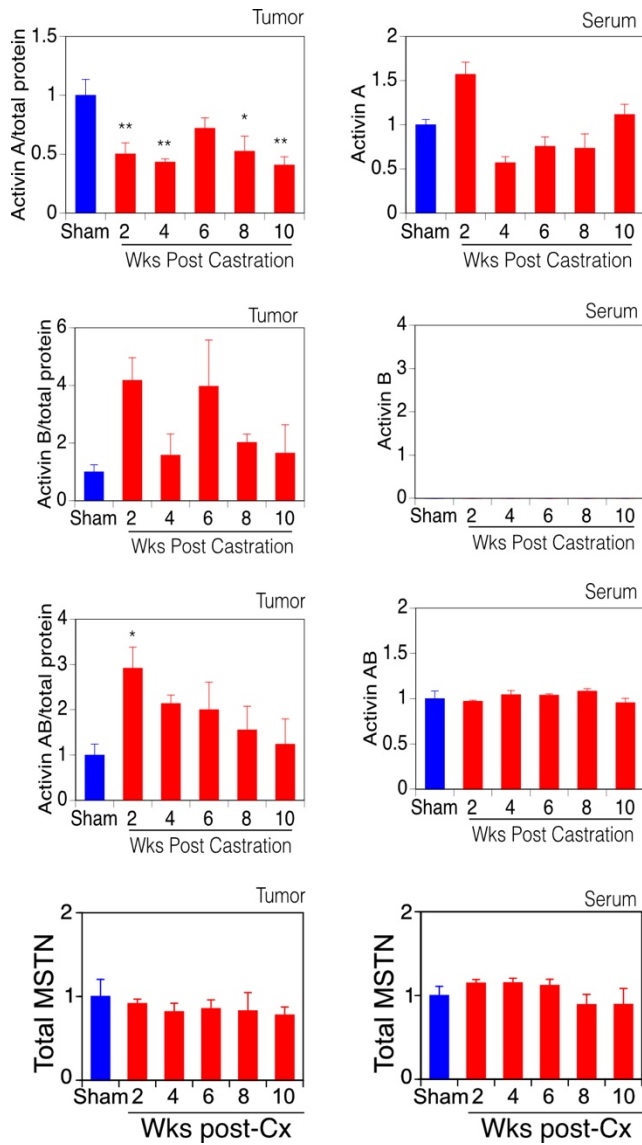


149
 150
 151 **Supplemental Figure S7. Additional data for TGFβ-family myokine ligand blockade treated cohorts of**
 152 **Fig. 4, including Sham-castrated/ActRIIB-Fc treated cohort and Total body mass. (A)** Grip strength after
 153 castration or sham-castration of mice treated with PBS, ActRIIB-Fc, or anti-GDF11 antibody. In addition to the
 154 indicated comparisons (green and purple asterisks), mice castrated and vehicle treated were also different (p
 155 < 0.001) from either sham castrated group from three weeks after castration. **(B)** Total body mass. **(C)**
 156 Individual skeletal muscle mass after 10 weeks castration by dissection and weighing. **(D)** Lean body mass by
 157 qNMR, as % of sham-castrated. Not indicated: Castration induced a significant reduction of each muscle mass
 158 and lean body mass ($p < 0.05$, blue versus red columns). ActRIIB-Fc treated groups were not different from
 159 each other. Mean (lines or columns), SEM (bars). $n = 3-5$ /group, * $p < 0.05$, ** $p < 0.01$, *** $p < 0.001$ for ActRIIB-
 160 Fc treated castrated (or anti-GDF11 treated castrated) versus vehicle treated castrated mice determined using
 161 two-way ANOVA with Tukey's HSD test.
 162



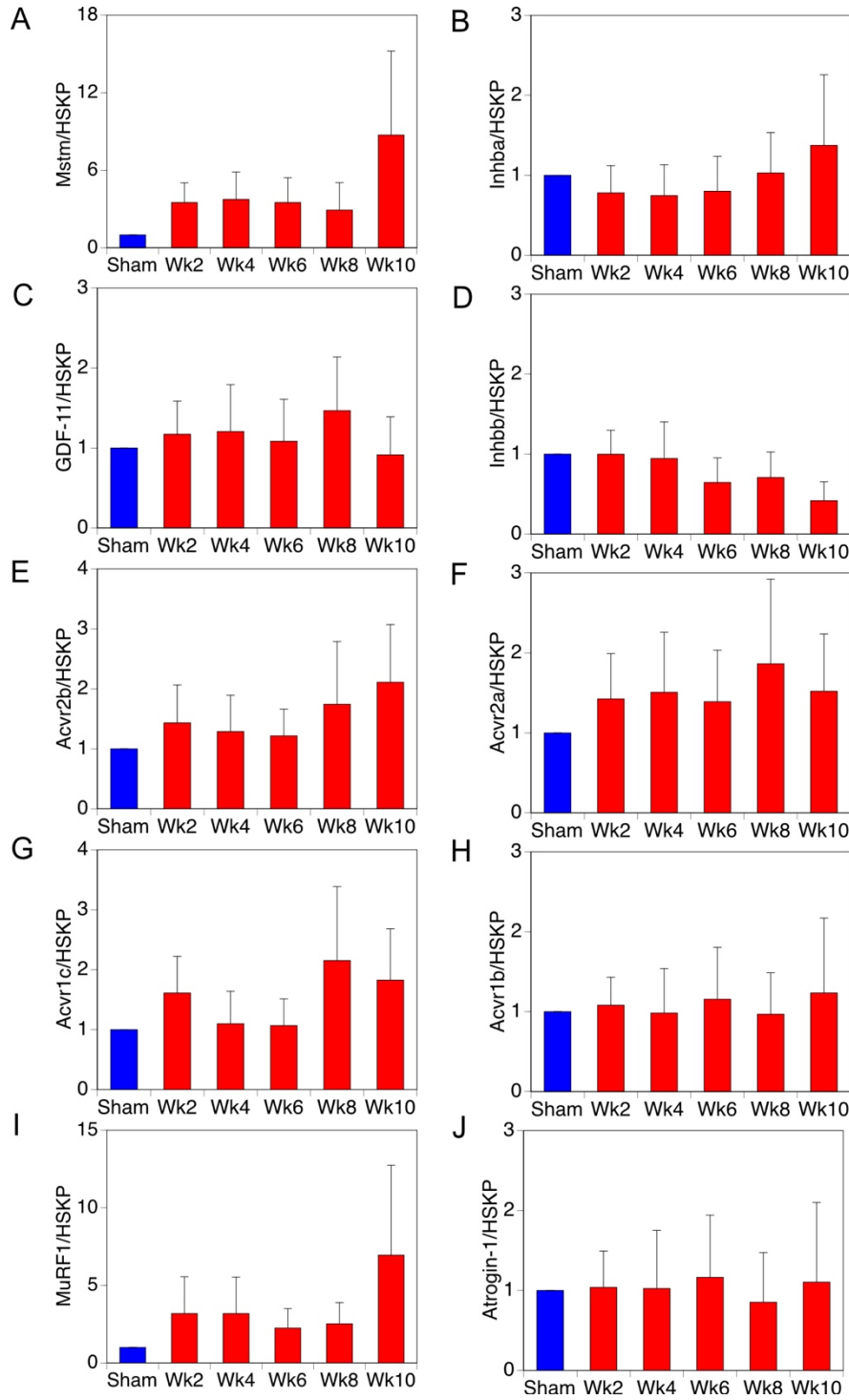
164
165
166
167
168
169
170
171
172
173
174
175
176
177
178

Supplemental Figure S8. Anti-GDF11 and anti-MSTN antibodies are sensitive and specific. (A) Immunoblot using anti-GDF11 (R&D #MAB19851) of an SDS-PAGE gel containing the indicated quantity of purified GDF11 and MSTN. (B) Immunoblot using anti-MSTN antibody (R&D #788-G8) of an SDS-PAGE gel containing the indicated quantity of purified MSTN and GDF11. (C) Immunoblot of GDF11 active dimer expression in the indicated quantity of mouse quadriceps (QUA) muscle extract. Right, quantitation of GDF11 active dimer expression versus total protein, $R^2 = 0.96$. (D) Immunoblot of MSTN active dimer expression in mouse quadriceps (QUA) muscle extract. Right, quantitation of MSTN active dimer expression versus total protein, $R^2 = 0.76$. E, Immunoblot of GDF11 active dimer expression in the indicated quantity of serum. Right, quantitation of GDF11 active dimer expression versus total protein, $R^2 = 0.99$. (F) Immunoblot of MSTN active dimer expression in the indicated quantity of serum. Right, quantitation of MSTN active dimer expression versus total protein, $R^2 = 0.99$.



180
 181
 182
 183
 184
 185
 186
 187
 188
 189
 190
 191
 192

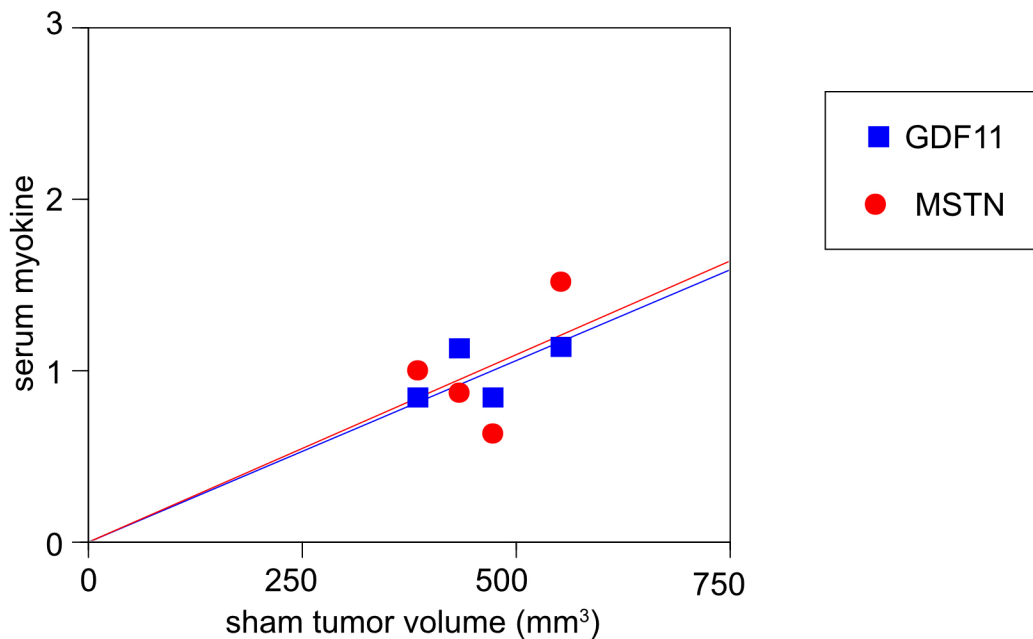
Supplemental Figure S9. Activins and total myostatin in tumor and serum after castration. ELISA determined levels of soluble, active activin A, Activin B, and Activin AB proteins, and total acid-solubilized myostatin (MSTN) in tumor and serum at the indicated time after castration. Activin B was not detected in serum. Mean protein levels after castration were normalized to sham-castrate group, from 4 mice at each time, measured 3 times.



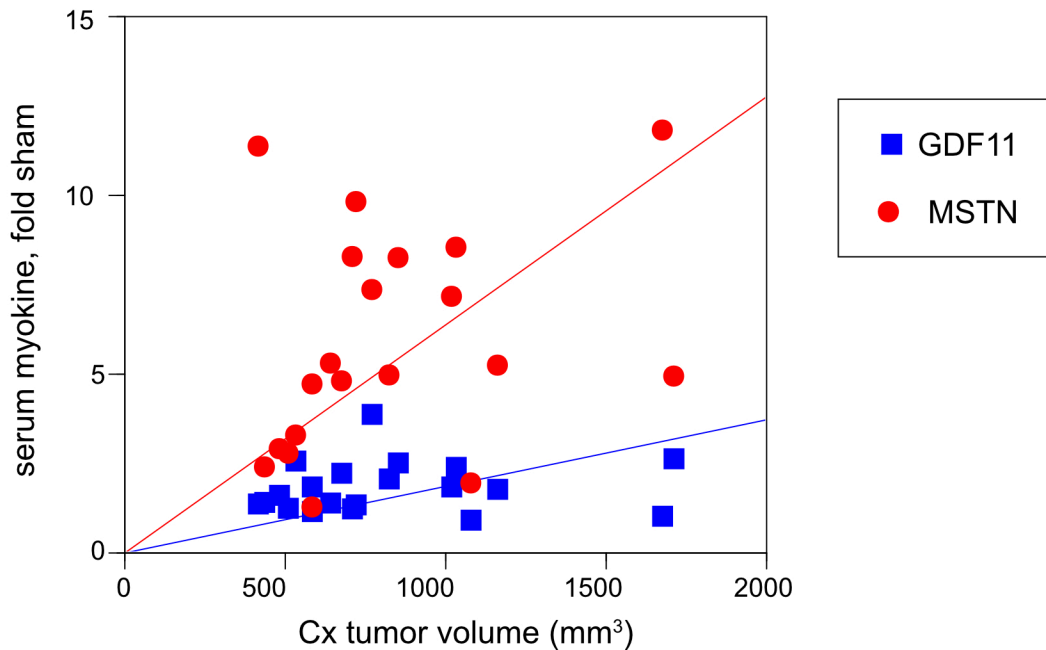
194
195
196
197
198
199
200
201
202

Supplemental Figure S10. Quantitation of catabolic TGF β -family myokine-related mRNAs in tumor. Expression of the indicated myokine associated mRNAs (A-J) from tumor tissue of PTEN prostate KO mice sacrificed at the indicated number of weeks after castration. Expression of each gene was normalized to control (HSKP) gene expression levels, and subsequently to the sham castrate expression levels, from 4 mice at each time, measured 3 times.

A



B



204

205

Supplemental Figure S11. Tumor volume predicted circulating GDF11 and myostatin protein levels.

207 ELISA determined soluble GDF11 levels or immunoblot determined soluble active myostatin levels plotted by

208 tumor volume (A) Myokines in serum of sham castrated animals in cohort #2 (n=4). Correlation for GDF11

209 $R^2=0.98$, $p=0.018$, MSTN $R^2=0.93$, $p=0.065$. (B) Myokines in serum at week of harvest for castrated (Cx)

210 animals in cohort #2 (n=20). Correlation for GDF11 $R^2=0.75$, $p<0.001$, MSTN $R^2=0.76$, $p<0.001$.

211

212